TTP08-26
March 6, 2009

Two-loop QED hadronic corrections to Bhabha scattering

Johann H. Kühn[1] and Sandro Uccirati[2]

Institut für Theoretische Teilchenphysik,
Universität Karlsruhe, 76128 Karlsruhe, Germany

Theoretical predictions for Bhabha scattering at the two-loop level require the inclusion of hadronic vacuum polarization in the photon propagator. We present predictions for the contributions from reducible amplitudes which are proportional to the vacuum polarization $\pi(q^2)$ and from irreducible ones where the vacuum polarization appears in a loop representing vertex or box diagrams. The second case can be treated by using dispersion relations with a weight function proportional to the R-ratio as measured in electron-positron annihilation into hadrons and kernels that can be calculated perturbatively. We present simple analytical forms for the kernels and, using two convenient parametrizations for the function $R(s)$, numerical results for the quantities of interest. As a cross check we evaluate the corresponding corrections resulting from light and heavy lepton loops and we find perfect agreement with previous calculations. For the hadronic correction our result are in good agreement with a previous evaluation.

Key words: Bhabha scattering, hadronic corrections, two-loop calculation.

PACS Classification: 12.20.Ds, 13.10.+q, 13.40,-f

[1]jk@particle.uni-karlsruhe.de
[2]uccirati@particle.uni-karlsruhe.de

1 Introduction

Electron-positron colliders, with their potential for precise and specific measurements of cross sections, have been and are being operated from the very low energy region around the pion threshold up to more than 200 GeV and may, in the future, reach up to energies of one or perhaps even several TeV. To determine the luminosity, one necessarily uses a reaction, whose cross section can be well measured and furthermore calculated with sufficient precision. Reactions which involve only leptons in the final state, like electron-positron annihilation into muon pairs or elastic electron-positron (Bhabha-)scattering are ideally suited for this purpose. In particular Bhabha scattering, with its relatively large cross section, has always been the standard luminosity monitor reaction. Precise theory predictions are, therefore, mandatory and, in view of recent interest in precise measurements with high counting rates, must be pushed to two-loop order.

Various ingredients are necessary in this connection. A major step has been made in [1] where the photonic two-loop virtual corrections plus the corresponding soft real radiation has been evaluated for the case of interest $m_e^2/s \ll 1$, using earlier results for the completely massless case [2] and exploiting the relation between the soft and collinear singularities for these two limiting cases. These results were confirmed in [3], where in addition also the contributions from muon loops (again in the limit $m_\mu^2/s \ll 1$) were calculated. These muon-loop contributions, in the same high-energy limit were also evaluated in [4], the corresponding results for arbitrary mass of the internal lepton were presented in [5]. The electron loop corrections involving the exact m_e^2/s dependence were computed in [6], while further efforts towards the full electron mass depedence at two-loop level can be found in [7].

All these contributions can be calculated strictly within Quantum Electrodynamics (we do not consider electroweak corrections that are relevant for high energies). However, in two loop approximation contributions from virtual hadrons come into play. From general considerations it is obvious that, generally speaking, their magnitude is comparable to or larger than those from virtual muons. It is well known [8] that these virtual hadronic contributions can be evaluated through dispersion relations, folding the absorptive part of the hadronic vacuum polarization, the R-ratio measured in electron-positron annihilation, with a kernel that can be calculated perturbatively, in the present case in a one-loop calculation. This approach has been adopted in [9], where the kernel for the box diagram has been calculated for non-vanishing electron mass and the limit $m_e \to 0$ has been considered only subsequently. A more compact form for this kernel can be obtained by using directly the well known results for the (direct plus crossed) box with one photon and one massive vector boson, the Z-γ box, contributing to Bhabha scattering at high energies. Since it is well known that in this case the electron mass can be safely set to zero from the beginning , the calculation becomes significantly simpler. Vertex corrections with a hadronic insertion have been evaluated with this technique long time ago and it is only this box contribution, that was not yet available since long.

As stated above, results for the hadronic contributions have been presented in [9]. In view of the fact, that we are using a somewhat different approach and furthermore, to provide an independent cross check the results of our calculation will be presented in some detail. To allow for an easier comparison with [9], we shall use the same parametrization [10] for the R-ratio. In addition we shall compare the results to the ones derived from a second parametrization [11] that includes more recent data and these latter ones should be considered as our definite predictions.

The paper will be organized as follows: In chapter 2 we present the general analysis and classify the various reducible and irreducible contributions. In chapter 3 we give the details of the calculation, the explicit forms of the kernels and identify the contributions from real radiation needed to render the results infrared finite. In this connection it is convenient to split the virtual (plus soft real) corrections into different building blocks that will be described in more detail in this chapter. The handling of the dispersion integrals with their poles is described in chapter 4. Of specific interest is the high energy limit, with s, t and u in an region where the R- ratio has approached an approximately constant value. In this limit and in analogy with the treatment on the form factor in [12] a particularly simple form can be derived where the information about hadron physics can be encoded into three "moments" of the R ratio. Using this method and evaluating the moments for a lepton, e.g. the muon or the tau-lepton, the results from [3] are easily recovered. In chapter 5 we present the numerical results for the two parametrizations. We give the results for the building blocks, vacuum polarization, vertex and boxes, and the complete corrections, split into the various contributions and discuss their physical relevance. The final Chapter 6 contains a brief summary and our conclusions.

2 General analysis

It is well known that contribution from the hadronic vacuum polarization can be directly evaluated by convoluting an appropriately chosen kernel with the familiar R-ratio ($R \equiv \sigma_{\rm had}/\sigma_{\rm pt}$) measured in electron-positron annihilation [8]. An arbitrary amplitude involving the hadronic vacuum polarization is obtained, by definition, from the original one by replacing the photon propagator as follows:

$$\frac{-\,ig_{\alpha\beta}}{q^2+i\epsilon} \quad\rightarrow\quad \frac{-\,ig_{\alpha\delta}}{q^2+i\epsilon}\, i\,(q^2 g^{\delta\epsilon}-q^{\delta}q^{\epsilon})\,\Pi(q^2)\,\frac{-\,ig_{\epsilon\beta}}{q^2+i\epsilon}. \tag{1}$$

The renormalized vacuum polarization function $\Pi(q^2)$ is obtained from its absorptive part (essentially the R-ratio) by the subtracted dispersion relation:

$$\Pi(q^2) = -\,\frac{q^2}{\pi}\int_{4m^2}^{\infty}\frac{dz}{z}\,\frac{{\rm Im}\Pi(z)}{q^2-z+i\epsilon}, \qquad {\rm Im}\Pi(z) = -\,\frac{\alpha}{3}\,R(z), \tag{2}$$

and has a cut for $q^2 > 4m^2$, with the threshold for hadron production at $4m^2$. The $q^{\delta}q^{\epsilon}$ term in Eq.(1) does not contribute and the photon propagator is effectively replaced as follows:

$$\frac{-\,ig_{\alpha\beta}}{q^2+i\epsilon} \quad\rightarrow\quad \frac{-\,ig_{\alpha\beta}}{q^2+i\epsilon}\Pi(q^2) = -\,ig_{\alpha\beta}\,\frac{\alpha}{3\pi}\int_{4m^2}^{\infty}\frac{dz}{z}\,\frac{R(z)}{q^2-z+i\epsilon}. \tag{3}$$

If q^2 is fixed by the external kinematics, applying the correction is equivalent to multiplication of the previous amplitude by $\Pi(q^2)$. In higher orders, summing the one-particle reducible terms only, this corresponds to the replacement of the photon propagator by the dressed one:

$$\frac{-\,ig_{\alpha\beta}}{q^2} \quad\rightarrow\quad \frac{-\,ig_{\alpha\beta}}{q^2}\,\frac{1}{1-\Pi(q^2)}. \tag{4}$$

However, if q stands for a loop momentum, it is convenient to exchange the order of integration and evaluate in a first step the loop integral with a ficticious massive vector boson of mass $\sqrt{z}$, and to convolute subsequently this amplitude with the R-ratio, i.e. with $\frac{\alpha}{3\pi}\int_{4m^2}^{\infty}\frac{dz}{z}R(z)$. In [12] this has been done for the Dirac form factor, assuming massless external fermions, and special emphasis has been put on the investigation of the limit, where the momentum transfer is far larger than $4m^2$. A similar approach will be useful for the present case. We will, in a first step, investigate the generic case valid for arbitrary $s, |t|, |u| \gg m_e^2$. The weight functions needed to obtain the three building blocks, namely the vacuum polarization function $\Pi(q^2)$ (Fig. 1a), the correction to the vertex function $V(q^2)$ (Fig. 1b) and the amplitude arising from the box diagrams (Fig. 1c), can be taken from the literature.

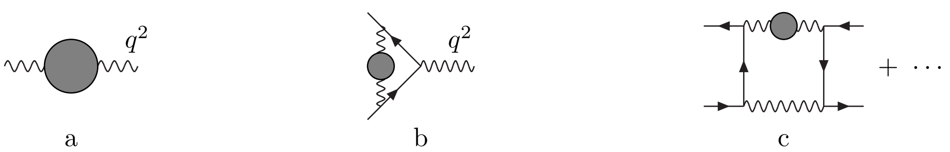

Figure 1: The building blocks for the QED hadronic corrections

The complete hadron induced corrections are conveniently split into thre classes:

1) Tree level diagrams, with two vacuum polarization insertions proportional to $\Pi(s)$ or $\Pi(t)$ where Π originates from virtual hadrons, muons or electrons (Fig. 2).

   These corrections to the amplitudes are proportional to $\Pi(s)^2$, $\Pi(t)^2$ or $\Pi(s)\Pi(t)$ (reducible quadratic Π-terms) and are directly obtained from the Born amplitude.

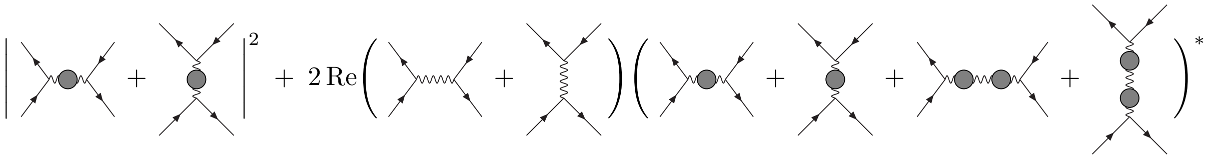

Figure 2: Tree level diagrams with vacuum polarization insertion

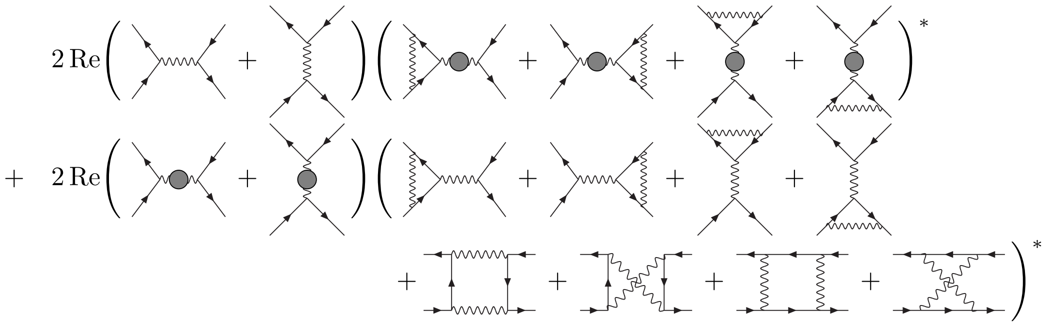

Figure 3: One-loop photonic diagrams in combination with a dressed photon propagator

2) Corrections which involve one-loop purely photonic corrections in combination with a dressed photon propagator in the s or t channel (Fig. 3).

   These are proportional to $\Pi(s)$ or $\Pi(t)$ (reducible linear Π-terms) and are directly obtained from the one-loop corrections to the Bhabha scattering. They can again be separated into amplitudes resulting from one-loop vertex and box corrections, respectively. Both are rendered infrared finite by adding soft real photon emission with $E_\gamma < \omega << \sqrt{s}$. In both cases this leads to a logarithmic ω-dependence.

   The photon vertex correction involves a collinear electron-mass singularity, which leads to the only m_e dependence relevant for our investigation.

   Also the $\gamma\gamma$-box amplitude, after interference with s- or t-channel dressed photon exchange, leads to a logarithmic dependence on ω. The electron mass, however, may safely be set to zero.

3) As a third class we have to consider the irreducible two-loop contributions, i.e. amplitudes with dressed photon propagator in a loop (Fig. 4).

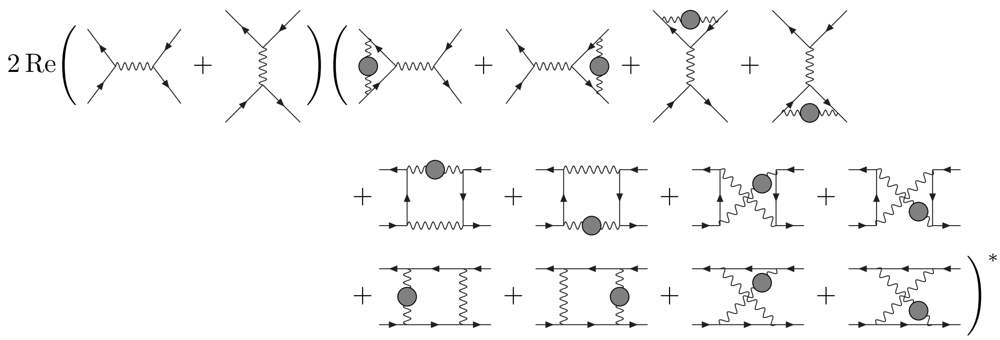

Figure 4: Irreducible two-loop diagrams

The dressed propagator may be located either in a vertex or in a box, which will interfere with the two Born amplitudes from s- and t-channel exchange. Irreducible vertex corrections are infrared finite and m_e may be safely set to zero. They are easily obtained from the Born amplitude by replacing the appropriate vertex by $V(s)$ or $V(t)$ as defined below. The box amplitudes are again infrared divergent and must be made finite by combining with soft real radiation.

Let us emphasize that contributions from lepton loops follow the same classification[1]. The simple form of the result in the high energy limit, $s, |t|, |u| \gg 4m_\pi^2$, will allow for a convenient cross check of our calculation.

In addition to these corrections with virtual photons, one has to compute the corresponding emission of real photons (Fig. 5) to compensate the infrared divergencies.

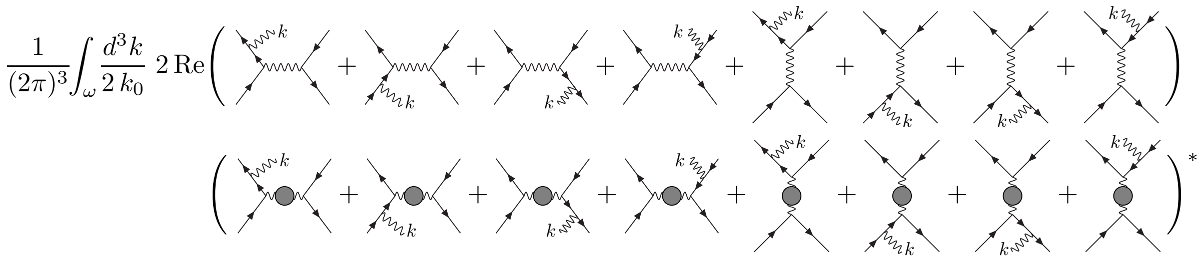

Figure 5: Diagrams with real photon emission. The four-momentum of the real soft photon is $k = (k_0, \vec{k})$ and the integration is performed for $|\vec{k}| < \omega$. Here and below infrared regularization through a small photon mass λ ($\lambda^2 = k_0^2 - \vec{k}^2$) is implicitly understood.

3 Details of the computation

In this section we discuss these contributions in details. In all equations containing products of Feynman diagrams,the sum over the spins of the outgoing particles and the average over the spins of the incoming particles is implicit, as well as the conservation of the external momenta. In these formulas, the coefficient $c_{PS} = (64 s \pi^2)^{-1}$ comes from the integration of the phase-space of the outgoing electron and positron.

3.1 Vacuum polarization insertion

The Born cross section is obtained from the combination of s- and t-channel exchange:

$$\frac{d\sigma^0}{d\Omega} = \frac{\alpha^2}{s}\left[\left(\frac{1}{2} - x + x^2\right) + \frac{1}{x^2}\left(1 - x + \frac{x^2}{2}\right) - \frac{1}{x}\left(1 - 2\,x + x^2\right)\right] = \frac{\alpha^2}{s}\left(\frac{1 - x + x^2}{x}\right)^2. \tag{5}$$

Replacing the photon propagator in the s- and t-channel by the dressed one, one obtains:

$$\frac{d\sigma^\Pi}{d\Omega} = \frac{\alpha^2}{s}\left\{\frac{1-2x+2x^2}{2}\left|\frac{1}{1-\Pi(s)}\right|^2 + \frac{2-2x+x^2}{2\,x^2}\left|\frac{1}{1-\Pi(t)}\right|^2 - \frac{1-2x+x^2}{x}\mathrm{Re}\frac{1}{[1-\Pi(s)]\,[1-\Pi(t)]}\right\}, \tag{6}$$

with $x = -t/s = (1 - \cos\theta)/2$ and

$$\Pi(q^2) = \Pi_e(q^2) + \Pi_\mu(q^2) + \Pi_\tau(q^2) + \Pi_{\mathrm{had}}(q^2). \tag{7}$$

[1]With the exception of the two-loop vacuum polarization (Fig. 6) whose absorptive part is in the hadronic case, by definition, part of the R-ratio.

Expanding up to order α^2, one easily recovers the Born contribution and the reducible one- and two-loop corrections:

$$\frac{d\sigma^{\Pi}}{d\Omega} = \frac{\alpha^2}{s}\left\{\frac{1-2x+2x^2}{2}\Big[1 + 2\mathrm{Re}\Pi(s) + 3(\mathrm{Re}\Pi(s))^2 - (\mathrm{Im}\Pi(s))^2\Big] + \frac{2-2x+x^2}{2\,x^2}\Big[1 + 2\Pi(t) + 3\Pi(t)^2\Big]\right.$$
$$\left. - \frac{1-2x+x^2}{x}\Big[1 + \mathrm{Re}\Pi(s) + \Pi(t) + (\mathrm{Re}\Pi(s))^2 - (\mathrm{Im}\Pi(s))^2 + \mathrm{Re}\Pi(s)\,\Pi(t) + \Pi(t)^2\Big]\right\}. \quad (8)$$

Using for light leptons (e and μ)

$$\Pi_l(s) = \frac{\alpha}{3\pi}\left[\left(\ln\frac{s}{m_l^2} - \frac{5}{3}\right) - i\pi\right], \qquad \Pi_l(t) = \frac{\alpha}{3\pi}\left(\ln\frac{-t}{m_l^2} - \frac{5}{3}\right), \qquad m_l = m_e, m_\mu, \quad (9)$$

the well known electron/muon induced one- and two-loop reducible contributions are easily recovered. In the present context the two-loop terms involving hadrons arise from terms proportional to Π^2_{had} and $\Pi_{\mathrm{had}}\Pi_{\mathrm{lept}}$, with different combinations of real and imaginary parts.

3.2 Reducible diagrams

Contributions from one-loop photonic amplitudes, interfering with amplitudes with the dressed photon propagator in the s- or t-channel are infrared divergent and must be combined with real radiation. For the amplitudes involving vertex corrections with have:

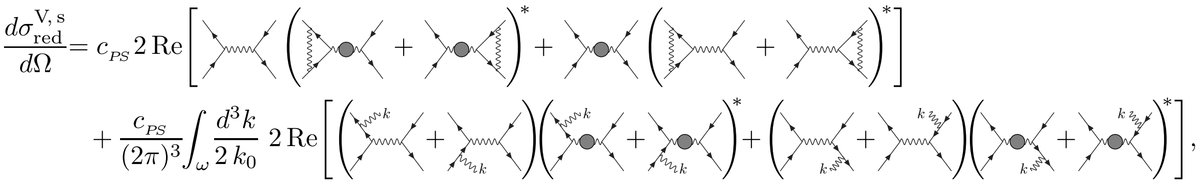

(10)

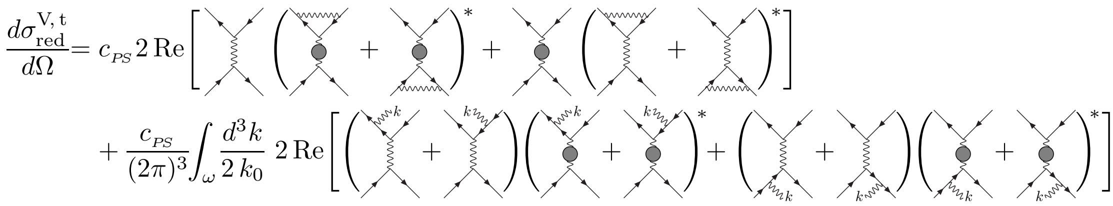

(11)

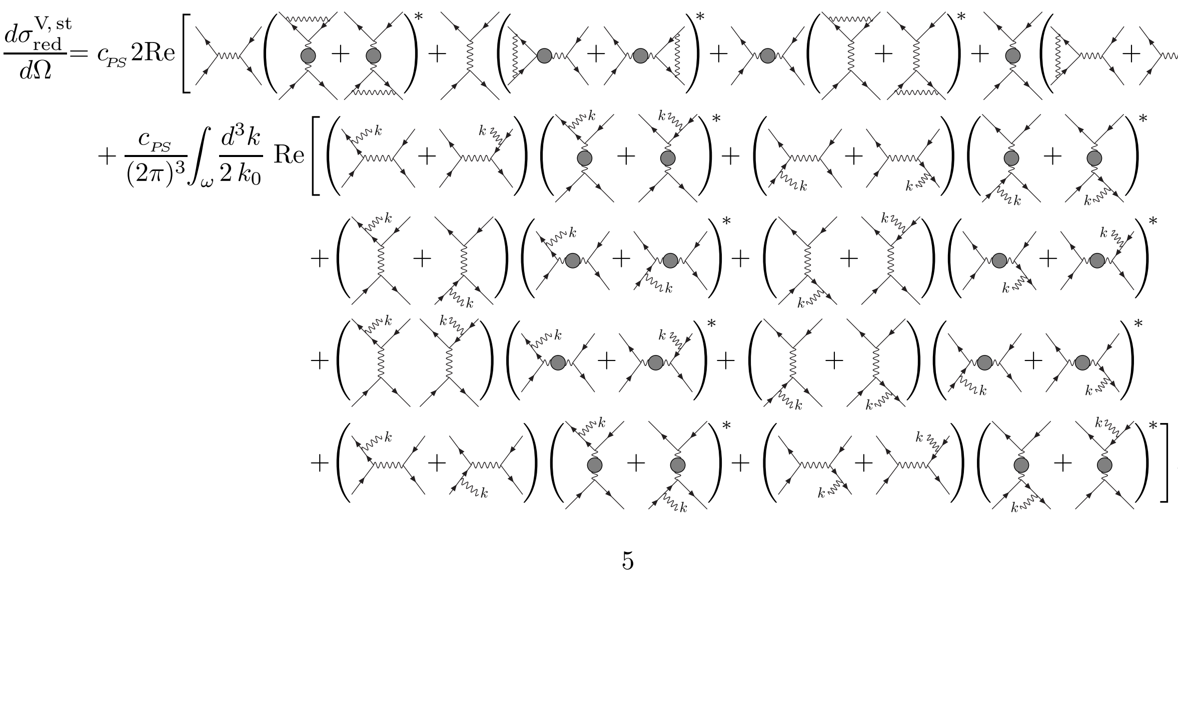

(12)

The sum of these three contributions from s-channel, t-channel and their interference gives the differential cross section:

$$\frac{d\sigma^{\rm V}_{\rm red}}{d\Omega} = \frac{\alpha^3}{s\pi}\Bigg\{ \frac{1-2x+2x^2}{2}\Big[4\,V_s^\gamma\,{\rm Re}\,\Pi(s)\Big] + \frac{2-2x+x^2}{2\,x^2}\Big[4\,V_t^\gamma\,\Pi(t)\Big] - \frac{1-2x+x^2}{x}\Big[(V_s^\gamma+V_t^\gamma)\Big({\rm Re}\,\Pi(s)+\Pi(t)\Big) + \pi\Big(\ln\frac{\lambda^2}{s}+\frac{3}{2}\Big)\,{\rm Im}\,\Pi(s)\Big]\Bigg\}, \tag{13}$$

where λ is the photon mass used as IR regulator. We have also introduced

$$V_s^\gamma = 2\ln\frac{2\omega}{\sqrt{s}}\Big(\ln\frac{s}{m_e^2}-1\Big)+\frac{3}{2}\ln\frac{s}{m_e^2}+2\,\zeta(2)-2,$$
$$V_t^\gamma = 2\ln\frac{2\omega}{\sqrt{s}}\Big(\ln\frac{-t}{m_e^2}-1\Big)+\frac{3}{2}\ln\frac{-t}{m_e^2}-\ln\frac{-t}{s}\ln\frac{-u}{s}-{\rm Li}_2\left(\frac{-t}{s}\right)-2. \tag{14}$$

Just like for the one-loop corrections, a logarithmic dependence on m_e from collinear singularities remains. It is interesting to notice the presence of an infrared divergent term proportional to ${\rm Im}\,\Pi(s)$ surviving after the inclusion of the real soft photon emission. Remembering that these contributions can be easily obtained from the $\mathcal{O}(\alpha)$ calculation it is clear that the $\mathcal{O}(\alpha)$ result is easily recovered by the substitution of $\Pi(s)$ and $\Pi(t)$ by 1.

A similar discussion applies to the photonic box diagrams, interfering with amplitudes with the dressed photon propagator in the s- or t-channel:

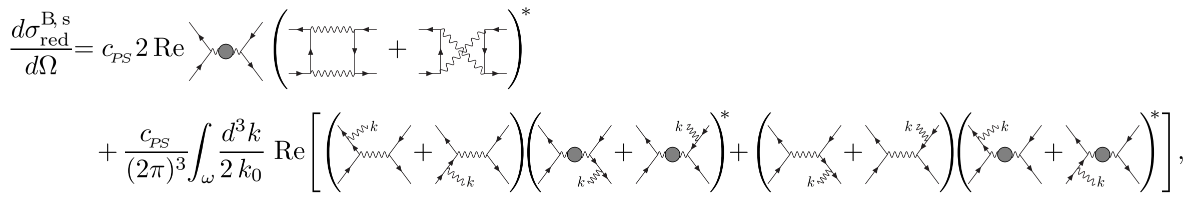
(15)

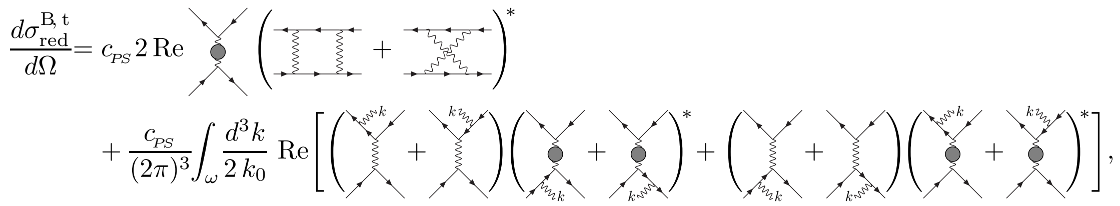
(16)

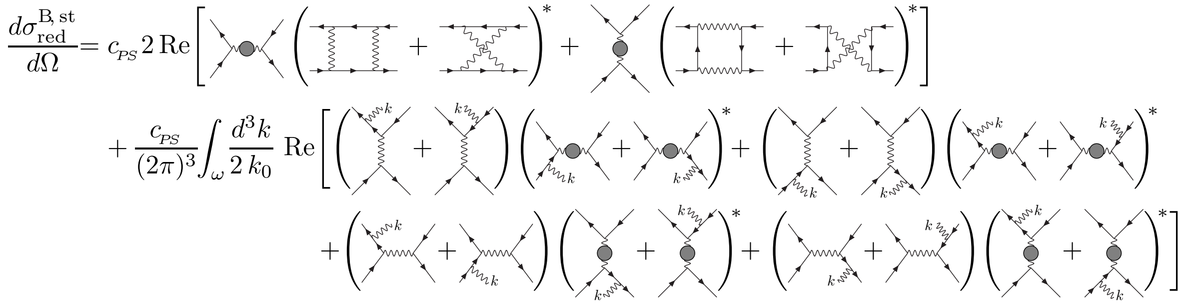
(17)

The differential cross section is then given by:

$$\frac{d\sigma^{\rm B}_{\rm red}}{d\Omega} = \frac{\alpha^3}{s\pi}\Bigg\{ \frac{1-2x+2x^2}{2}\left[2\,B_s^\gamma\,\mathrm{Re}\,\Pi(s) + 2\pi\ln\frac{t}{u}\,\mathrm{Im}\,\Pi(s)\right] - \mathrm{Re}\left[\Big(B^\gamma(s,t)-B^\gamma(s,u)\Big)\,\Pi^*(s)\right]$$
$$+\frac{2-2x+x^2}{2\,x^2}\left[2\,B_t^\gamma\,\Pi(t)\right] - \mathrm{Re}\left[\Big(B^\gamma(t,s)-B^\gamma(t,u)\Big)\,\Pi(t)\right]$$
$$-\frac{1-2x+x^2}{x}\left[B_t^\gamma \mathrm{Re}\Pi(s) + B_s^\gamma\Pi(t) - \pi\,\ln\frac{\lambda^2}{-t}\,\mathrm{Im}\Pi(s)\right] + \mathrm{Re}\left[xB^\gamma(t,s)\Pi^*(s) + \frac{1}{x}B^\gamma(s,t)\Pi(t)\right]\Bigg\}, \tag{18}$$

where we have introduced

$$\begin{aligned} B_s^\gamma &= 2\ln\frac{2\omega}{\sqrt{s}}\ln\frac{t}{u} + \frac{1}{2}\ln^2\frac{-t}{s} - \frac{1}{2}\ln^2\frac{-u}{s} - \ln\frac{-t}{s}\ln\frac{-u}{s} - 2\,\mathrm{Li}_2\left(\frac{-t}{s}\right) + \zeta(2), \\ B_t^\gamma &= -2\ln\frac{2\omega}{\sqrt{s}}\ln\frac{-u}{s} - \frac{1}{2}\ln^2\frac{-u}{s} + \ln\frac{-t}{s}\ln\frac{-u}{s} - \mathrm{Li}_2\left(\frac{-t}{s}\right), \\ B^\gamma(a,b) &= -\frac{a+b}{2\,a}\ln\frac{b}{a+i\,\epsilon} + \frac{a+2b}{4\,a}\left(\ln^2\frac{b}{a+i\,\epsilon} + \pi^2\right). \end{aligned} \tag{19}$$

In this case the electron mass can be safely set to zero. Also in this case a logarithm of λ^2 survives and cancels exactly the one generated by the vertex reducible corrections, rendering the total cross section infrared finite.

3.3 Irreducible diagrams

Let us move to the third group consisting of the two irreducible contributions. The vertex correction has been discussed in detail in [12] and can be cast into the following form:

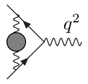

$$\Longrightarrow \qquad V(q^2) = \frac{\alpha}{3\pi}\int_{4m^2}^{\infty}\frac{dz}{z}R(z)\rho(q^2,z-i\epsilon), \tag{20}$$

with

$$\rho(q^2,z) = -\frac{7}{8} - \frac{z}{2q^2} + \frac{1}{2}\left(\frac{3}{2}+\frac{z}{q^2}\right)\ln\frac{-z}{q^2} + \frac{1}{2}\left(1+\frac{z}{q^2}\right)^2\left[\zeta(2) - \mathrm{Li}_2\left(1+\frac{z}{q^2}\right)\right]. \tag{21}$$

The contribution to the cross section can be cast into a form closely related to the Born cross section.

$$\frac{d\sigma^{\rm V,\,s}}{d\Omega} = c_{PS}\,2\,\mathrm{Re}$$

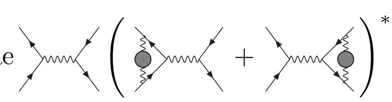

$$\frac{d\sigma^{\rm V,\,t}}{d\Omega} = c_{PS}\,2\,\mathrm{Re}$$

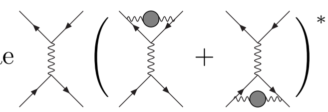

$$\frac{d\sigma^{\rm V,\,st}}{d\Omega} = c_{PS}\,2\,\mathrm{Re}$$

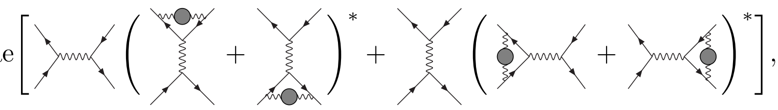

$$\tag{22}$$

$$\frac{d\sigma^{\rm V}}{d\Omega} = \frac{\alpha^3}{s\,\pi}\left\{\frac{1-2x+2x^2}{2}\Big[4\,\mathrm{Re}\,V(s)\Big] + \frac{2-2x+x^2}{2\,x^2}\Big[4\,V(t)\Big] - \frac{1-2x+x^2}{x}\Big[2\,V(t) + 2\,\mathrm{Re}\,V(s)\Big]\right\}. \tag{23}$$

As stated above, m_e has been set to zero and the result is obviously infrared finite.

Finally for the irreducible two-loop box contributions the kernels can again be directly taken from the literature [13]. The part of the kernel, which corresponds to the infrared divergent piece will be canceled by the proper combination of real soft radiation amplitudes which are also proportional to $\Pi(q^2)$, specifically:

$$\frac{d\sigma^{\rm B,\,s}}{d\Omega} = c_{PS}\,2\,\mathrm{Re}$$

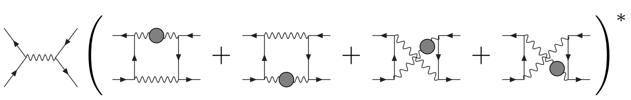

$$+\frac{c_{PS}}{(2\pi)^3}\int_\omega \frac{d^3k}{2\,k_0}\,\mathrm{Re}$$

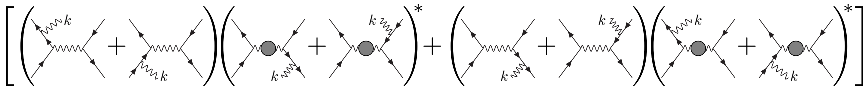

$$\tag{24}$$

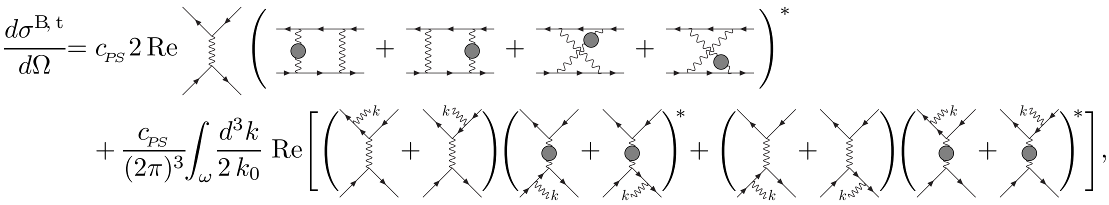

(25)

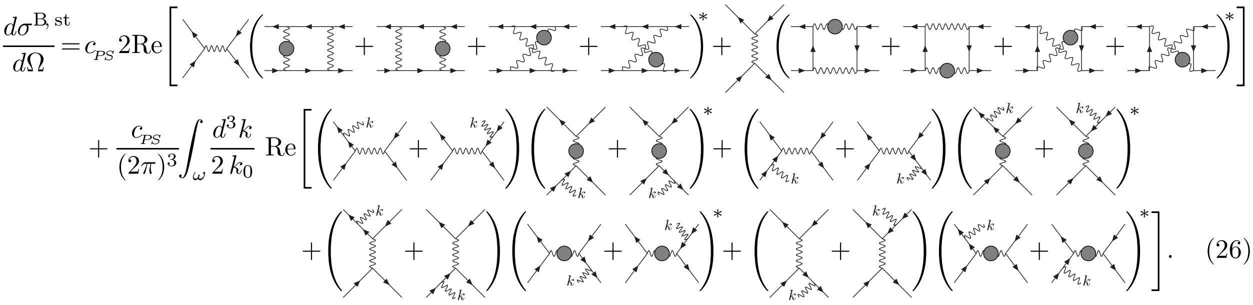

(26)

In total we find:

$$\frac{d\sigma^{\mathrm{B}}}{d\Omega} = \frac{\alpha^3}{s\pi}\Bigg\{ \frac{1-2x+2x^2}{2}\Big[2\,B_s\,\mathrm{Re}\,\Pi(s)\Big] - \mathrm{Re}\Big[B(s,t,u)-B(s,u,t)\Big]$$
$$+\frac{2-2x+x^2}{2\,x^2}\Big[2\,B_t\,\Pi(t)\Big] - \mathrm{Re}\Big[B(t,s,u)-B(t,u,s)\Big]$$
$$-\frac{1-2x+x^2}{x}\Big[B_t\,\mathrm{Re}\,\Pi(s)+B_s\,\Pi(t)\Big] + \mathrm{Re}\Big[x\,B(t,s,u)+\frac{1}{x}\,B(s,t,u)\Big]\Bigg\}, \tag{27}$$

where

$$B_s = 2\ln\frac{2\omega}{\sqrt{s}}\ln\frac{t}{u} - \ln\frac{-t}{s}\ln\frac{-u}{s} - 2\,\mathrm{Li}_2\left(\frac{-t}{s}\right) + \zeta(2), \qquad B_t = -2\ln\frac{2\omega}{\sqrt{s}}\ln\frac{-u}{s} - \mathrm{Li}_2\left(\frac{-t}{s}\right) + 3\,\zeta(2), \tag{28}$$

and

$$B(a,b,c) = B_A(a,b,c) + B_B(a,b,c), \qquad B_j(a,b,c) = \frac{\alpha}{3\pi}\int_{4m^2}^{\infty}\frac{dz}{z}R(z)\,\xi_j(a,b,c,z-i\epsilon), \qquad j = A,B; \tag{29}$$

$$\xi_A(a,b,c,z) = \frac{c^2}{a\,(z-a)}\left[2\ln\frac{c}{b+i\epsilon}\ln\left(1-\frac{a}{z}\right) - \mathrm{Li}_2\left(1+\frac{b}{z}\right) + \mathrm{Li}_2\left(1+\frac{c}{z}\right)\right],$$
$$\xi_B(a,b,c,z) = \frac{c}{a}\left[\left(\frac{z}{a}-1\right)\ln\left(1-\frac{a}{z}\right) + \ln\frac{-b}{z}\right] + \frac{c-b-z}{a}\left[\ln\frac{b+i\epsilon}{-a}\ln\left(1-\frac{a}{z}\right) - \mathrm{Li}_2\left(1-\frac{a}{z}\right) + \mathrm{Li}_2\left(1+\frac{b}{z}\right)\right].$$

The part proportional to $\ln(2\omega/\sqrt{s})$ has been displayed separately and, as stated before, is proportional to $\Pi(s)$ or $\Pi(t)$. As discussed in the introduction, the functions ξ_A and ξ_B, corresponding to the box diagram with a massive and a massless vector boson, can be directly read off from the literature [13].

For the two-loop hadronic contributions to cross section we find (without the trivial vacuum polarization)

$$
\begin{aligned}
\frac{d\sigma_{\rm had}}{d\Omega} &= \frac{d\sigma^{\rm V}_{\rm red}}{d\Omega} + \frac{d\sigma^{\rm B}_{\rm red}}{d\Omega} + \frac{d\sigma^{\rm V}}{d\Omega} + \frac{d\sigma^{\rm B}}{d\Omega} \\
&= \frac{\alpha^3}{s\pi}\Bigg\{\frac{1-2x+2x^2}{2}\left[2\left(2\,V_s^\gamma + B_s^\gamma + B_s\right)\mathrm{Re}\,\Pi(s) + 2\,\pi\ln\frac{t}{u}\,\mathrm{Im}\,\Pi(s) + 4\,\mathrm{Re}\,V(s)\right] \\
&\quad + \frac{2-2x+x^2}{2\,x^2}\left[2\left(2\,V_t^\gamma + B_t^\gamma + B_t\right)\Pi(t) + 4\,V(t)\right] \\
&\quad - \frac{1-2x+x^2}{x}\Bigg[\left(V_s^\gamma + V_t^\gamma + B_t^\gamma + B_t\right)\mathrm{Re}\,\Pi(s) + \left(V_s^\gamma + V_t^\gamma + B_s^\gamma + B_s\right)\Pi(t) \\
&\qquad + \pi\left(\ln\frac{-t}{s} + \frac{3}{2}\right)\mathrm{Im}\,\Pi(s) + 2\,V(t) + 2\,\mathrm{Re}\,V(s)\Bigg] \\
&\quad - \mathrm{Re}\Bigg[\left(B^\gamma(s,t) - B^\gamma(s,u) + \frac{t}{s}B^\gamma(t,s)\right)\Pi^*(s) + \left(B^\gamma(t,s) - B^\gamma(t,u) + \frac{s}{t}B^\gamma(s,t)\right)\Pi(t) \\
&\qquad - \frac{u}{t}\,B(s,t,u) - B(s,u,t) - \frac{u}{s}B(t,s,u) - B(t,u,s)\Bigg]\Bigg\}. \qquad (30)
\end{aligned}
$$

4 Evaluation of the dispersion integrals

In Eq.(30), the total cross section is written in terms of the building blocks $\Pi(q^2)$, $V(q^2)$ and $B(a,b,c)$ defined in Eq.(2), Eq.(20) and Eq.(29) respectively. In the hadronic case, given a suitable parametrization of $R(s)$, these dispersion integrals have to be integrated numerically. Therefore, before attempting the evaluation of the cross section, all sources of numerical instability must be cured.

The expression for $\Pi(q^2)$ in Eq.(2) is very simple, but reveals the presence of a pole of the integrand at $z = q^2 + i\epsilon$. The simplest way to get rid of it is to add and subtract $R(q^2)$ in the integrand for $q^2 > 0$ (s-channel). After the useful change of variable $z = 4m^2/y$, we get:

$$
\Pi(t) = \frac{\alpha}{3\pi}\int_0^1 dy\frac{t}{yt-4m^2}R\left(\frac{4m^2}{y}\right), \qquad \Pi(s) = \frac{\alpha}{3\pi}\left\{\ln\left(1-\frac{s}{4m^2-i\epsilon}\right)R(s) + \int_0^1 dy\frac{s}{ys-4m^2}\left[R\left(\frac{4m^2}{y}\right) - R(s)\right]\right\}. \quad (31)
$$

The integral for $V(q^2)$ given in Eq.(20) does not show any pole in the integration domain and is directly accessible to a numerical evaluation. However, its convergence in the high energy integration region can be improved introducing the asymptotic, approximately constant value $R(\infty)$ of the R-ratio. To this purpose, let us recall the results from [12] for the vertex V, which can be rewritten in the form:

$$
V(q^2) = \frac{\alpha}{3\pi}\left\{R(\infty)\int_0^1\frac{dy}{y}\rho\,(q^2,\frac{4m^2}{y}) + \int_0^1\frac{dy}{y}\rho\,(q^2,\frac{4m^2}{y})\left[R\left(\frac{4m^2}{y}\right) - R(\infty)\right]\right\}. \qquad (32)
$$

The first one of these integrals can be solved exactly:

$$
\begin{aligned}
I_\rho(r) = \int_0^1\frac{dy}{y}\rho(q^2,\frac{4m^2}{y}) &= -\frac{1}{12}\ln^3(-r) - \ln(-r)\left[\zeta(2) + \frac{7}{8} + \frac{1}{4r} + \frac{1}{2}\mathrm{Li}_2\left(-\frac{1}{r}\right)\right] \\
&\quad + \left(\frac{3}{4} + \frac{1}{r} + \frac{1}{4r^2}\right)\left[\zeta(2) - \mathrm{Li}_2(1+r)\right] + \frac{15}{16} + \frac{1}{4r} - \mathrm{Li}_3\left(-\frac{1}{r}\right), \qquad (33)
\end{aligned}
$$

where $r = q^2/(4m^2 - i\epsilon)$, and the second integral converges well in the large momentum region.

A similar approach can be adopted for integrating the kernel from the box diagram $B(a,b,c)$ defined in Eq.(29). The function ξ_A has a good high energy behaviour, but has a pole (for $a = s > 0$) in $z = a + i\epsilon$ and can be treated in the same way as $\Pi(q^2)$:

$$B_A(t,b,c) = \frac{\alpha}{3\pi} \int_0^1 \frac{dy}{y}\, \xi_A(t,b,c,\frac{4m^2}{y})\, R\Big(\frac{4m^2}{y}\Big),$$

$$B_A(s,b,c) = \frac{\alpha}{3\pi} \left\{ R(s) \int_0^1 \frac{dy}{y}\, \xi_A(s,b,c,\frac{4m^2}{y}) + \int_0^1 \frac{dy}{y}\, \xi_A(s,b,c,\frac{4m^2}{y}) \Big[R\Big(\frac{4m^2}{y}\Big) - R(s) \Big] \right\}. \tag{34}$$

The first integral in the expression for $B_A(s,b,c)$ is then given by:

$$I_A(s,b,c) = \int_0^1 \frac{dy}{y} \xi_A(s,b,c,\frac{4m^2}{y}) = \frac{c^2}{s^2} \left[\ln \frac{c}{b+i\epsilon} \ln^2 \frac{4m^2-s}{4m^2} + J_A\Big(-\frac{b}{s}\Big) - J_A\Big(-\frac{c}{s}\Big) \right], \tag{35}$$

where

$$\begin{aligned} J_A(x) = & \frac{1}{6}\ln^3(-xr) + \frac{1}{6}\ln^3\frac{xr}{-\bar{r}} - \frac{1}{2}\ln x \ln^2(-xr) - \frac{1}{2}\ln(\bar{x}r)\ln^2(1-\bar{x}r) + \frac{1}{2}\ln\frac{1-\bar{x}r}{x}\ln^2\frac{xr}{-\bar{r}} \\ & - \ln\bar{r}\,\mathrm{Li}_2(1-\bar{x}r) + \ln\frac{xr}{-\bar{r}}\,\mathrm{Li}_2\Big(\frac{\bar{r}\bar{x}}{-x}\Big) + \ln(\bar{x}r)\Big[\mathrm{Li}_2(r) - \mathrm{Li}_2(\bar{x}r) - \mathrm{Li}_2\Big(\frac{xr}{1-\bar{x}r}\Big)\Big] \\ & + \ln(-xr)\Big[\mathrm{Li}_2(r) - \mathrm{Li}_2(\bar{x}r) - \mathrm{Li}_2\Big(\frac{-\bar{x}}{x}\Big)\Big] - \mathrm{Li}_3\Big(\frac{-\bar{x}}{x}\Big) + \mathrm{Li}_3(\bar{x}r) + \mathrm{Li}_3\Big(\frac{\bar{r}\bar{x}}{-x}\Big) + S_{12}\Big(\frac{1-\bar{x}r}{\bar{r}}\Big). \end{aligned} \tag{36}$$

In the last expression we have introduced $\bar{x} = 1-x$, $r = s/(4m^2 - i\epsilon)$, $\bar{r} = 1-r$. On the other hand, B_B can be computed following the same procedure used for $V(q^2)$:

$$B_B(a,b,c) = \frac{\alpha}{3\pi} \left\{ R(\infty) \int_0^1 \frac{dy}{y}\, \xi_B(a,b,c,\frac{4m^2}{y}) + \int_0^1 \frac{dy}{y}\, \xi_B(a,b,c,\frac{4m^2}{y}) \Big[R\Big(\frac{4m^2}{y}\Big) - R(\infty) \Big] \right\}. \tag{37}$$

where for the first integral we have:

$$\begin{aligned} I_B(a,b,c) = & \int_0^1 \frac{dy}{y} \xi_B(a,b,c,\frac{4m^2}{y}) \\ = & \frac{c}{a}\left[\mathrm{Li}_2\Big(\frac{a}{4m^2}\Big) - \ln\frac{-b}{4m^2}\right] + \frac{c-b}{a}\left\{ \ln\frac{-b}{4m^2}\Big[\mathrm{Li}_2\Big(\frac{-b}{4m^2}\Big) - \mathrm{Li}_2\Big(\frac{a}{4m^2}\Big)\Big] + 2\,\mathrm{Li}_3\Big(\frac{a}{4m^2}\Big) - 2\,\mathrm{Li}_3\Big(\frac{-b}{4m^2}\Big) \right\} \\ & + \frac{4m^2-a}{a}\left[\Big(\ln\frac{-b}{4m^2} - \frac{c}{a}\Big)\ln\frac{4m^2-a}{4m^2} + \mathrm{Li}_2\Big(\frac{a}{4m^2}\Big)\right] - \frac{4m^2+b}{a}\left[\ln\frac{-b}{4m^2}\ln\frac{4m^2+b}{4m^2} + \mathrm{Li}_2\Big(\frac{-b}{4m^2}\Big)\right]. \end{aligned} \tag{38}$$

4.1 High energy limit

In the high energy limit, i.e. for $\sqrt{s}$ and $\sqrt{-t}$ far larger than the energy above which $R(s)$ approaches (sufficiently rapidly) $R(\infty)$, the building blocks $\Pi(q^2)$, $V(q^2)$ and $B(a,b,c)$ can be expressed in terms of the moments R_n defined through:

$$R_n = \int_0^1 \frac{dx}{x} \frac{\ln^n x}{n!} \Big[R\Big(\frac{4m^2}{x}\Big) - R(\infty) \Big]. \tag{39}$$

The large q^2 behaviour of the vacuum polarization is then given by:

$$\Pi(q^2) = \frac{\alpha}{3\pi} \Big(R(\infty) \ln \frac{-q^2}{4m^2 - i\epsilon} + R_0 \Big), \tag{40}$$

and V takes the following form:

$$V(q^2) = \frac{\alpha}{3\pi} \left\{ R(\infty) I_\rho(r) + R_0 \Big[-\frac{1}{4}\ln^2(-r) + \frac{3}{4}\ln(-r) - \zeta(2) - \frac{7}{8} \Big] + R_1 \Big[-\frac{1}{2}\ln(-r) + \frac{3}{4} \Big] - \frac{1}{2} R_2 \right\},$$

$$I_\rho(r) = -\frac{1}{12}\ln^3(-r) + \frac{3}{8}\ln^2(-r) - \Big[\zeta(2) + \frac{7}{8}\Big]\ln(-r) + \frac{3}{2}\zeta(2) + \frac{15}{16} + \mathcal{O}(|r|^{-1}). \tag{41}$$

Similarly, the building block $B(a,b,c)$, in the high energy limit $s, |t|, |u| \gg 4\,m^2$ is given by:

$$B(a,b,c) = \frac{\alpha}{3\pi}\Bigg\{R(\infty)\, I_\xi(a,b,c) + R_0\left[\frac{c^2}{a^2}L_{b\,c}\left(\ln\frac{-a}{4m^2}-\frac{L_b+L_c}{2}\right)-\frac{c-b}{2a}\left(L_b^2+6\zeta(2)\right)+\frac{c}{a}L_b\right]+R_1\frac{c^2}{a^2}L_{b\,c}\Bigg\}, \quad (42)$$

where

$$I_\xi(a,b,c) = \frac{c^2}{a^2}\left\{L_{b\,c}\left[\frac{1}{2}\ln^2\frac{-a}{4m^2}-\frac{1}{2}\ln\frac{-a}{4m^2}\,(L_b+L_c)+\zeta(2)\right]-J(b,c)+J(c,b)\right\}$$
$$-\frac{c-b}{2a}\left[L_b^2+6\zeta(2)\right]\left(\ln\frac{-a}{4m^2}-1+\frac{L_b}{3}\right)+\frac{c}{a}\left[L_b\left(\ln\frac{-a}{4m^2}-1\right)-\frac{L_b^2}{2}-5\,\zeta(2)\right]+\mathcal{O}(m^2). \quad (43)$$

In the last equations we have introduced:

$$L_b = \ln\frac{b+i\epsilon}{a}, \qquad L_c = \ln\frac{c+i\epsilon}{a}, \qquad L_{b\,c} = \ln\frac{b+i\epsilon}{c}, \qquad J(x,y) = S_{12}\left(\frac{-x}{y-i\epsilon}\right)+i\,\pi\,\mathrm{Li}_2\left(\frac{-x}{y-i\epsilon}\right). \quad (44)$$

4.2 The leptonic contribution

With these ingredients the two-loop result induced by massive and light leptons is easily recovered.

$$\frac{d\sigma_l}{d\Omega} = \frac{d\sigma^{\mathrm{V}}_{\mathrm{red},\,l}}{d\Omega}+\frac{d\sigma^{\mathrm{B}}_{\mathrm{red},\,l}}{d\Omega}+\frac{d\sigma^{\mathrm{V}}_{l}}{d\Omega}+\frac{d\sigma^{\mathrm{B}}_{l}}{d\Omega}. \quad (45)$$

All ingredients are obtained from the corresponding expressions for the hadronic case using the R-ratio:

$$R_l(z) = \left(1+\frac{4m_l^2}{2\,z}\right)\sqrt{1-\frac{4m_l^2}{z}}. \quad (46)$$

Numerical evaluations for the muon and τ-lepton will be presented below. In the high energy limit we will use the moments [12]:

$$R_l(\infty) = 1, \qquad R_{l,0} = \ln 4-\frac{5}{3}, \qquad R_{l,1} = \frac{1}{2}\ln^2 4-\frac{5}{3}\ln 4+\frac{28}{9}-\zeta(2),$$
$$R_{l,2} = \frac{1}{6}\ln^3 4-\frac{5}{6}\ln^2 4+2\left[\frac{28}{9}-\zeta(2)\right]\ln 4+2\zeta(3)+\frac{5}{3}\zeta(2)-\frac{164}{27}. \quad (47)$$

The integral over z can then be analytically evaluated, giving for the building blocks:

$$\Pi_l(q^2) = -\frac{\alpha}{3\pi}\left(\ln\frac{-q^2}{m_l^2}-\frac{5}{3}\right),$$
$$V_l(q^2) = -\frac{\alpha}{3\pi}\left\{\frac{1}{12}\ln^3\frac{-q^2}{m_l^2}-\frac{19}{24}\ln^2\frac{-q^2}{m_l^2}+\frac{1}{2}\left[\zeta(2)+\frac{265}{36}\right]\ln\frac{-q^2}{m_l^2}+\zeta(3)-\frac{19}{12}\zeta(2)-\frac{3355}{432}\right\},$$
$$B_l(a,b,c) = -\frac{\alpha}{3\pi}\Bigg\{-\frac{c^2}{a^2}\left[\frac{1}{2}L_{b\,c}\left(\ln^2\frac{-a}{m^2}-\ln\frac{-a}{m^2}\left(L_b+L_c+\frac{10}{3}\right)+\frac{5}{3}\left(L_b+L_c\right)+\frac{56}{9}\right)-J(b,c)+J(c,b)\right]$$
$$+\frac{c-b}{2a}\left[L_b^2+6\,\zeta(2)\right]\left(\ln\frac{-a}{m_l^2}-\frac{8}{3}+\frac{1}{3}L_b\right)-\frac{c}{a}\left[L_b\left(\ln\frac{-a}{m_l^2}-\frac{8}{3}\right)-\frac{1}{2}L_b^2-5\,\zeta(2)\right]\Bigg\}, \quad (48)$$

where L_b, L_c, $L_{b\,c}$ and $J(x,y)$ were defined in Eq.(44). In the previous formula the $i\epsilon$ prescription is implicit in the squared lepton mass ($m_l^2 \to m_l^2 - i\epsilon$) and gives the rule to extract the proper imaginary part of the logarithms. For electron loops the vertex correction differs by a constant [14]:

$$V_e(q^2) = -\frac{\alpha}{3\pi}\left[\frac{1}{12}\ln^3\frac{-q^2}{m_e^2}-\frac{19}{24}\ln^2\frac{-q^2}{m_e^2}+\frac{1}{2}\left[\zeta(2)+\frac{265}{36}\right]\ln\frac{-q^2}{m_e^2}+\frac{3}{4}\zeta(2)-\frac{383}{36}\right], \quad (49)$$

the remaining corrections are identical.

In order to obtain the total leptonic corrections, the contributions of the one- and two-loop vacuum polarization function have to be added:

$$\frac{d\sigma_l^{\rm tot}}{d\Omega} = \frac{d\sigma_l}{d\Omega} + \frac{d\sigma_l^{\Pi}}{d\Omega} + \frac{d\sigma_l^{\rm S}}{d\Omega}. \tag{50}$$

The second term can be obtained from Eq.(2) with the substitution $\Pi \to \Pi_l$, while last term can be computed taking from the literature the expression for the leptonic contribution to the two-loop vacuum polarization function (Fig. 6):

$$\frac{d\sigma_l^{\rm S}}{d\Omega} = \frac{\alpha^2}{s}\left\{\frac{1-2x+2x^2}{2}\left[2\,{\rm Re}\Pi_l^{(2)}(s)\right] + \frac{2-2x+x^2}{2\,x^2}\left[2\,\Pi_l^{(2)}(t)\right] - \frac{1-2x+x^2}{x}\left[{\rm Re}\Pi_l^{(2)}(s) + \Pi_l^{(2)}(s)\right]\right\},$$

where in the high-energy limit[2]

$$\Pi_l^{(2)}(q^2) = \frac{\alpha^2}{4\pi^2}\left[\ln\frac{-\,q^2}{m_l^2 - i\epsilon} - \frac{5}{6} + 4\,\zeta(3)\right]. \tag{51}$$

Comparing our analytical result with [3], we find perfect agreement.

$$\frac{d\sigma_l^{\rm S}}{d\Omega} = c_{PS}\, 2\, {\rm Re}$$

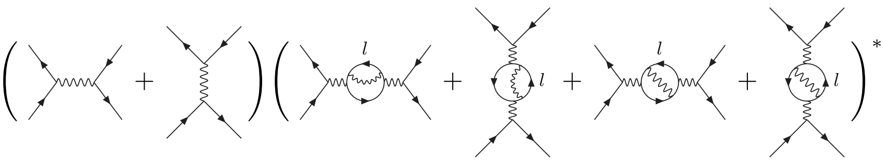

Figure 6: Contributions involving the two-loop vacuum polarization from a lepton l.

5 Numerical analysis

To arrive at a numerical result we adopt the following parametrizations for $R(s)$: For the comparison with earlier work [9] we take the function provided by H.Burkhardt [10]. This parametrization (denoted by B) is simple and efficient for the integration, however, it includes only data more than 20 years old. A newer parametrization (denoted by HMNT) is based on the most recent and accurate data and will be used for most of our detailed predictions. The two parametrizations for $R(s)$ are shown in Fig. 7.

The contributions from narrow resonances are incorporated using:

$$R_{\rm res}(s) = \frac{9\pi}{\alpha^2(M_{\rm res})} M_{\rm res}\Gamma_{e^+e^-}\,\delta(s - M_{\rm res}^2). \tag{52}$$

For the parametrization HMNT we take J/Ψ, $\psi(2S)$, $\Upsilon(1S)$, $\Upsilon(2S)$ and $\Upsilon(3S)$ as narrow resonances with the parameters listed in Table 1, thus replacing their rapidly varying cross section governed by a narrow Breit-Wigner shape with an easy to be integrated delta function. Parametrization B uses slightly different

	J/Ψ	$\Psi(2S)$	$\Upsilon(1S)$	$\Upsilon(2S)$	$\Upsilon(3S)$
M(GeV)	3.096916(11)	3.686093(34)	9.46030(26)	10.02326(31)	10.3552(5)
Γ_{ee}(keV)	5.55(14)	2.48(6)	1.340(18)	0.612(11)	0.443(8)
$(\alpha/\alpha(M))^2$	0.957785	0.95554	0.932069	0.93099	0.930811

Table 1: Masses and electronic widths of the narrow resonances and effective electromagnetic coupling at the appropriate scales.

[2]For general $m_l^2/|q^2|$ the result can be found in [15]

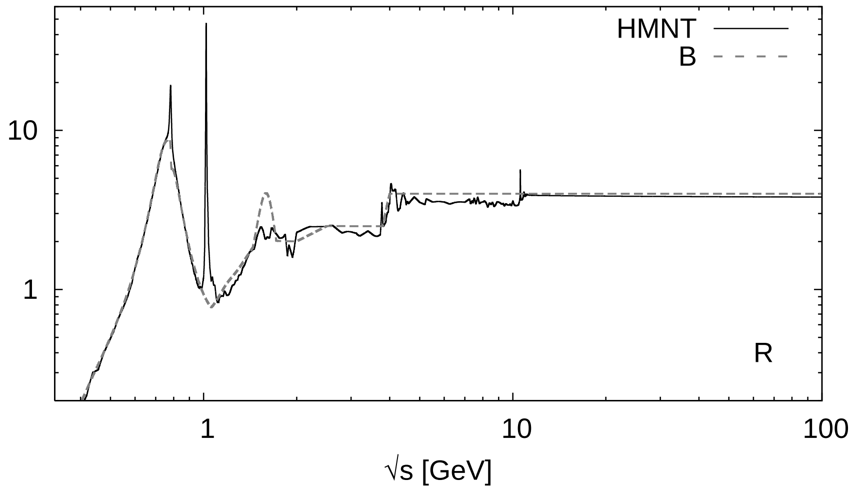

Figure 7: The two parametrization B (dashed) and HMNT (solid) for $R(s)$ without narrow resonances.

values and includes in addition $\omega(782)$, $\Phi(1020)$, $\psi(3770)$, $\psi(4040)$, $\psi(4160)$, $\psi(4415)$, $\Upsilon(4S)$, $\Upsilon(10860)$ and $\Upsilon(11020)$ as narrow resonances and we adopt the parameter values listed in the code [10]. For later use we also give the results for the moments $R(\infty)$, R_0, R_1 and R_2 based on parametrization B:

$$R(\infty) = 4.0, \qquad R_0 = -8.31, \qquad R_1 = 13.1, \qquad R_2 = -15.6. \tag{53}$$

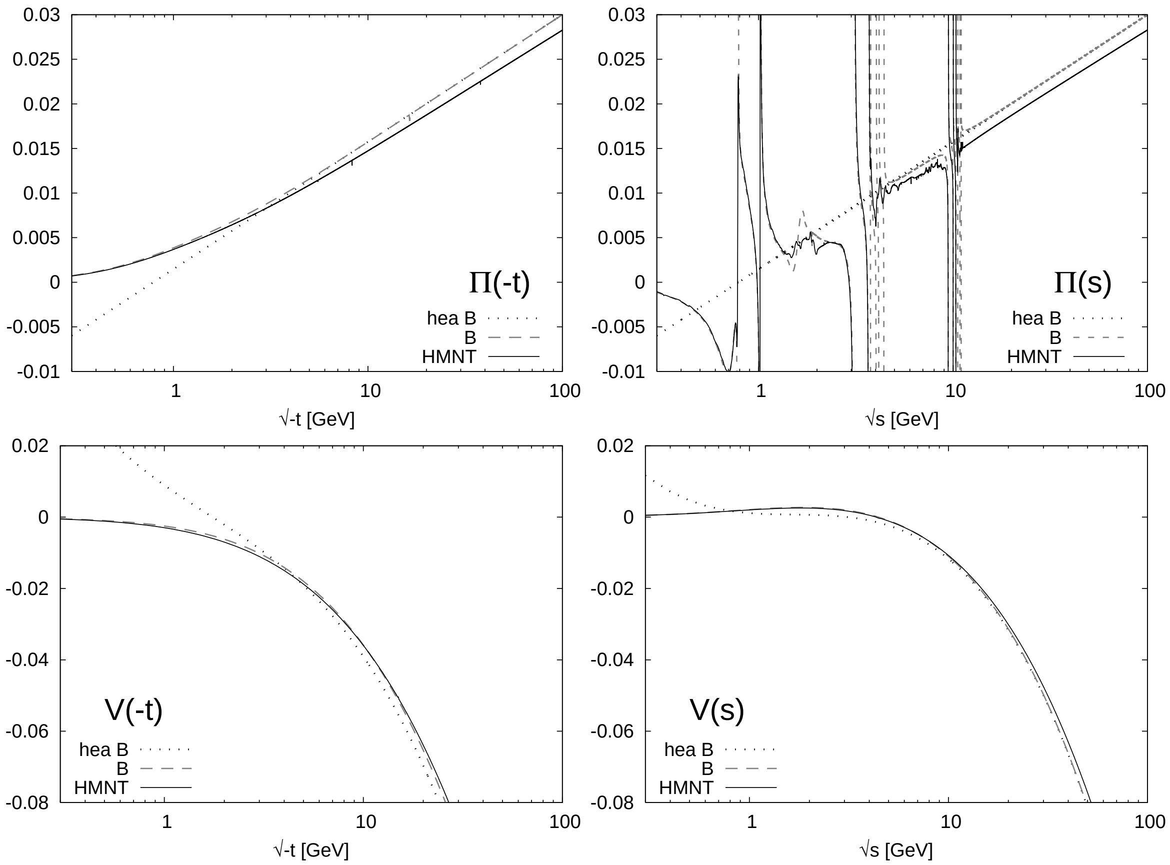

Figure 8: Vacuum polarization $\Pi(q^2)$ and vertex correction $V(q^2)$ for spacelike (-t) and timelike (s) momenta for the parametrizations B (dashed) and HMNT (solid) and the high energy approximation (dotted)

The results for the vacuum polarization $\Pi(q^2)$ and the vertex correction $V(q^2)$ for space-like and time-like q^2 are shown in Fig. 8 as functions of q^2. We display the predictions based on both parametrization B (dashed) and HMNT (solid). For comparison we also show the behaviour in the high energy approximation (dotted) of eq.(40-41), for parametrization B only. As expected from the comparison in Fig. 7, the difference between the two parametrization leads to differences in $\Pi(q^2)$ and $V(q^2)$ of less than 10% which are unimportant for the two-loop analysis (the present uncertainty for HMNT amounts to typically one to two percent). For $\Pi(t)$ and $V(q^2)$ the high energy approximation starts to deviate significantly from the full result for energies below 3 GeV, while for $\Pi(s)$ the resonant behaviour cannot be reproduced by this approximation. The corresponding results for the functions $B(a, b, c)$, which govern the behaviour of the irreducible box contribution are shown in Fig. 9 for a set of representative energies as functions of the scattering angle θ. The result for $B(s, u, t)$ is obtained from $B(s, t, u)$ through the substitution $\cos\theta \to -\cos\theta$.

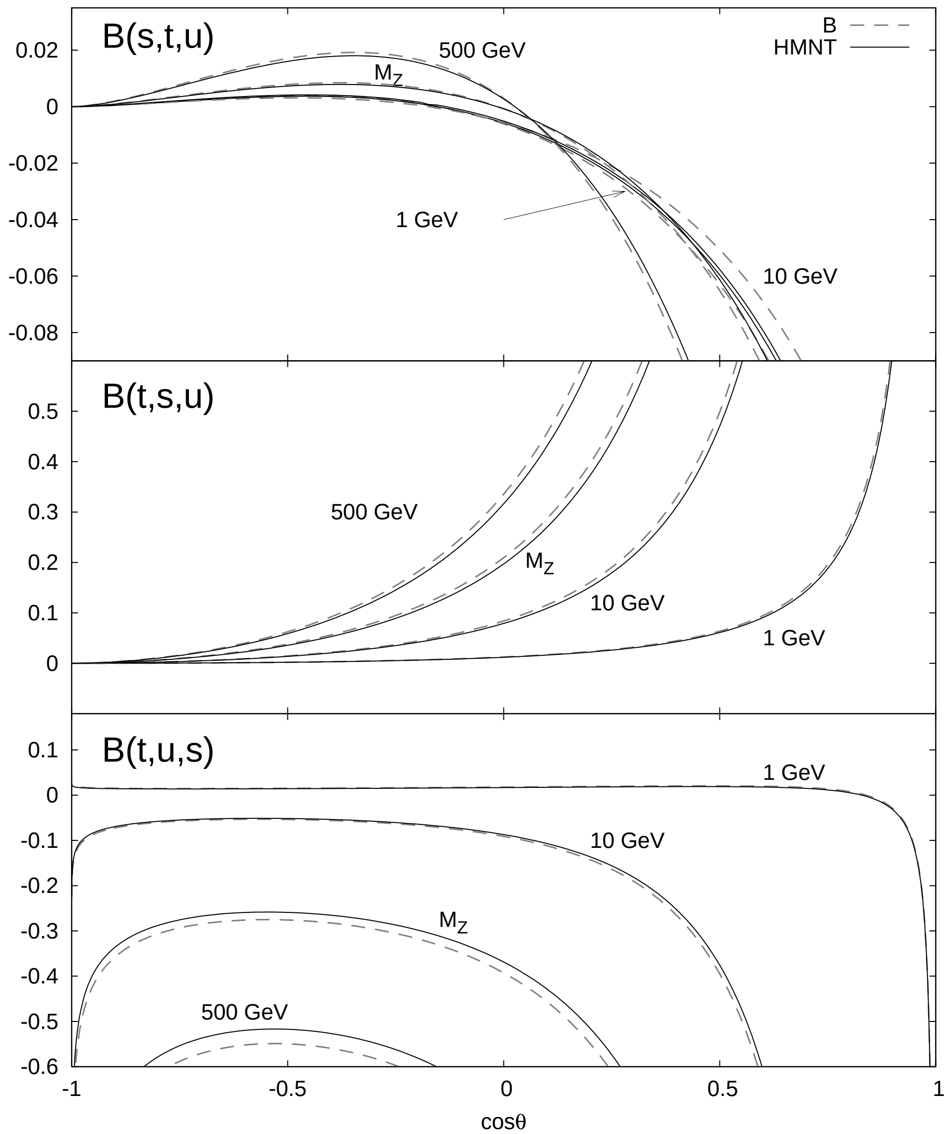

Figure 9: The functions B(a,b,c) defined in Eq.(29) for different kinematical regions versus $\cos\theta$ using the parametrizations B (dashed) and HMNT (solid).

As expected, the predictions for Π, V and B based on the two paratrizations B and HMNT are always quite close, hence the following discussion will be based on HMNT only.

The corrections for the differential distributions are shown in Fig. 10 for four characteristic energies, normalized relative to the Born prediction[3]. They are separated into those from reducible diagrams ($d\sigma^{\rm red} = d\sigma^{\rm V}_{\rm red} + d\sigma^{\rm B}_{\rm red}$), irreducible vertex ($d\sigma^{\rm V}$) and box ($d\sigma^{\rm B}$) diagrams[4]. In most of the cases the reducible ones are significantly larger than the irreducible ones, a consequence of their enhancement by the large logarithm $\ln(s/m_e^2)$.

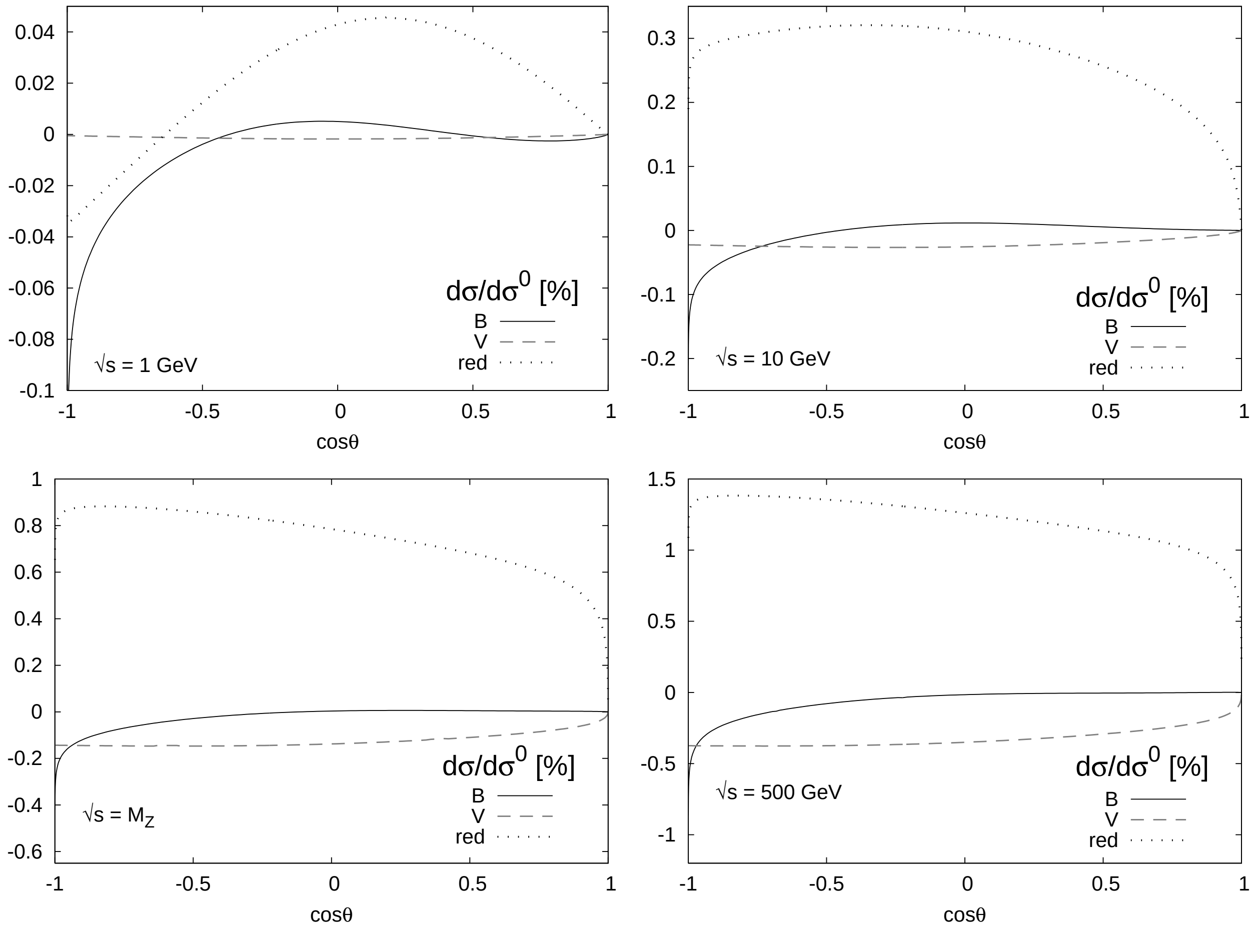

Figure 10: Relative corrections to the cross section from irreducible boxes $d\sigma^B$ (solid), vertices $d\sigma^V$ (dashed) and reducible contribution $d\sigma^{\rm red} = d\sigma^B_{\rm red} + d\sigma^V_{\rm red}$ (dotted) for four characteristic energies using parametrization HMNT.

In Fig. 11 we display the corresponding contributions from muons (solid line) and τ leptons (dashed line), which can be evaluated similar to the hadronic ones. It is interesting to observe that the high energy approximation (hea) for the muon case, $m_\mu^2 \ll s, |t|, |u|$, (dotted) fails quite badly for small angles at $\sqrt{s} = 1$ GeV, a fact that could be anticipated already from Fig. 8, which shows the pour quality of this approximation for $\sqrt{-t} < 3$ GeV in the hadronic case. For high energies, the quality of the approximation should be sufficient for all practical purposes (Fig. 11).

[3]We do not present the two-loop vacuum polarization insertions of Eq.(8) which are best combined with the one-loop and Born contribution in the resummed form of Eq.(6). It is clear that $\Pi_{\rm had}(q^2)$ must be known with a relative precision of about one percent, if one aims at luminosity determination with an error significantly below one per mille.

[4]Here and below the infrared-sensitive contributions proportional to $\ln(2\omega/\sqrt{s})$ are set to zero.

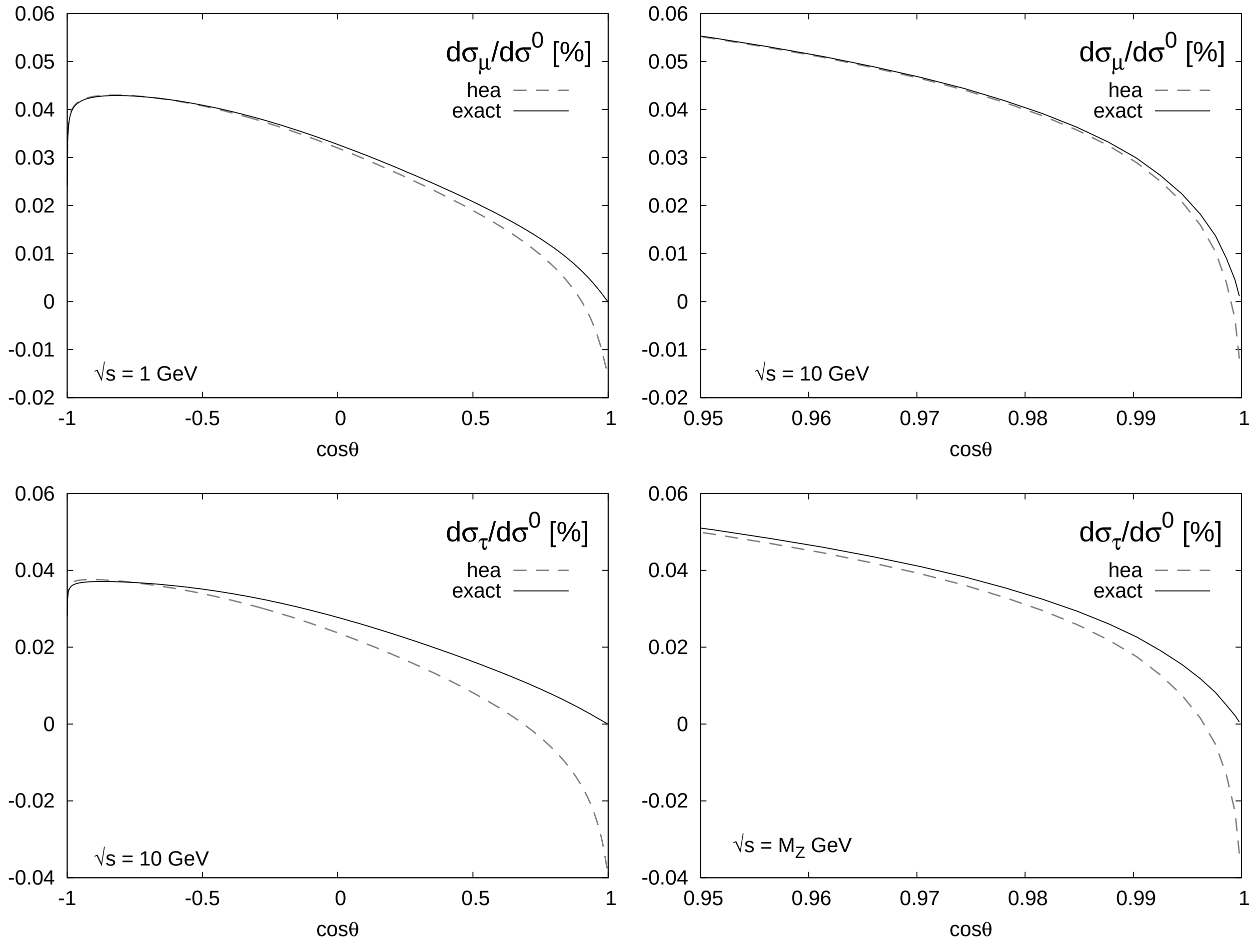

Figure 11: Leptonic cross section $d\sigma_l$ from muons (upper) and τ-leptons (lower) (Eq.(45)) relative to the Born cross section. Comparison is shown between the high energy approximation (hea) of Eq.(48) (dashed) and the exact result (solid) obtained from numerical integration using R_l as defined in Eq.(46).

The relative corrections from hadron and lepton (e, μ, τ) loops are compared in Fig. 12. A markedly different energy and angular dependence is observed for the four contributions. Individually and in the sum, they significantly exceed the level of one per mille necessary to achieve the corresponding precision of the luminosity measurements. However, as discussed before, the reducible terms dominate and the irreducible hadronic terms are typically below one per mille. For precise comparisons the numerical results are also listed in Table 2 for a selected set of energies and angles. For small angles the box contribution $d\sigma^B$ remains tiny, often around or below 10^{-5} of the Born cross section, and the result is dominated by the reducible correction $d\sigma^{\rm red}$ which is typically a factor 10 to 100 larger and is trivially obtained from existing one-loop results, Eq.(13)-(18).

To illustrate the relative importance of reducible and irreducible contributions, the results for the irreducible box $d\sigma^B$ and the sum $d\sigma^{B+\rm red} = d\sigma^B + \sigma^{\rm red}$ are listed in Table 3. The relative contribution of $d\sigma^B$ is evidently tiny. The results for $d\sigma^{B+\rm red}$ are also compared with those from [9]. For the hadronic case they are in good agreement, although sometimes deviating in the last of the digits listed in [9]. For the leptons perfect agreement is observed.

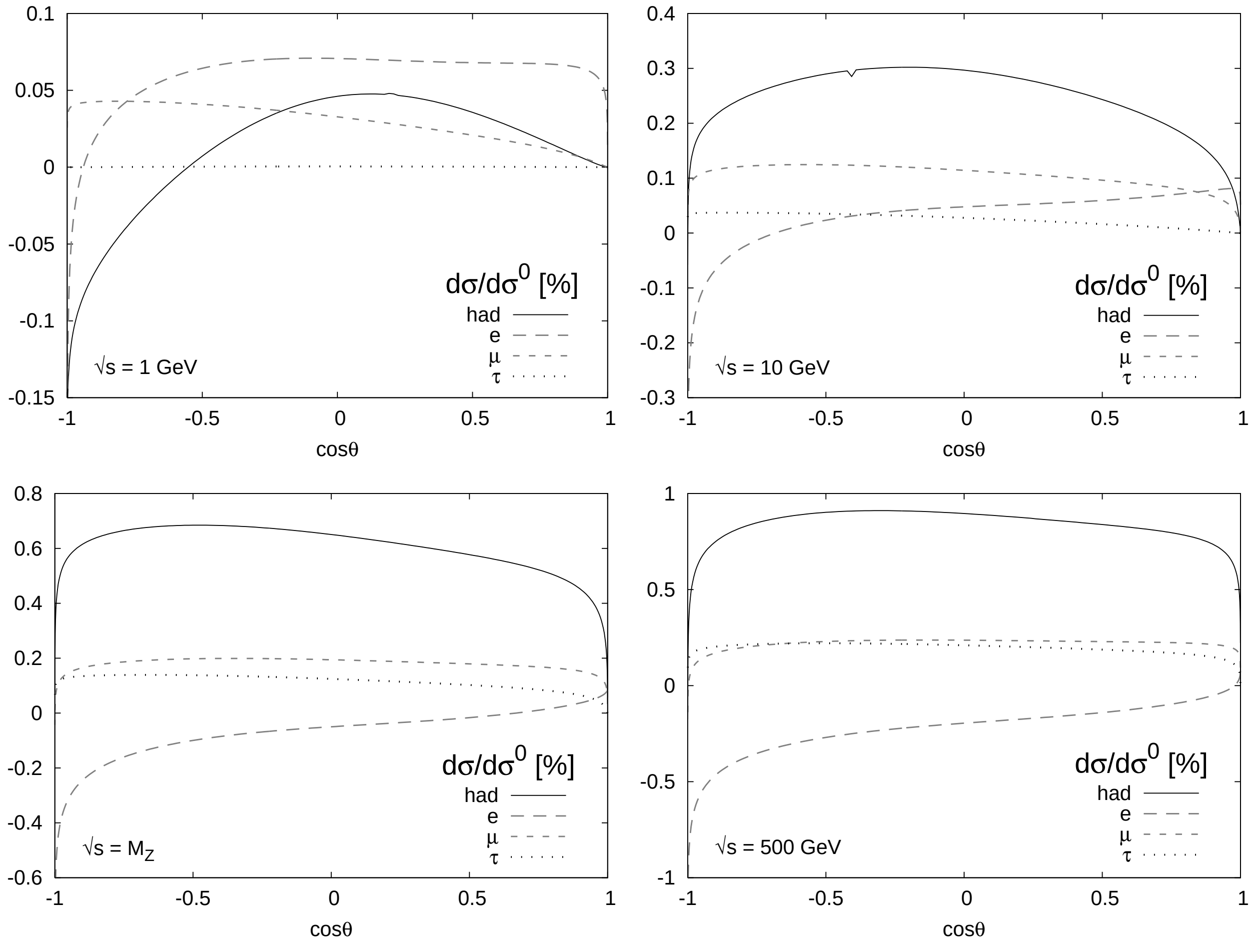

Figure 12: Relative corrections from hadron and lepton loops as functions of $\cos\theta$ for four characteristic energies. The high energy approximation of Eq.(48) is used for electron contribution at all energies and for muons for $\sqrt{s} \geq 10$ GeV.

In general, the corrections exhibit a fairly smooth energy dependence. However, the situation changes for energies close to narrow resonances. This is exemplified in Fig. 13 for two cases: around the Φ and around the J/Ψ resonances for three fixed angles: 3^o, 90^o and 177^o. The interference of the continuum amplitude with a Breit-Wigner enhanced correction is clearly visible. At 3^o (177^o), irreducible box and the reducible corrections are of comparable size and opposite (equal) sign, at 90^o the reducible ones dominate. The vertex corrections are always small. Formally for the case of the J/Ψ, treated as narrow resonance, the correction even diverges, and it is still extremely large if the natural width of J/Ψ is introduced. In practice, however, the cross section has to folded with the energy spread of order MeV. In this case the singular amplitude with its asymmetric behaviour around $\sqrt{s} = M_{\rm res}$ is damped and thus remains a small correction. From these considerations, it is clear that a precise parametrization of $R(s)$ is required in regions of rapidly varying cross section, if one aims at a precise prediction of the corrections in this region.

$\sqrt{s}$	1 GeV			10 GeV		
θ	3^o	90^o	177^o	3^o	90^o	177^o
$d\sigma^0/d\Omega$ [pbarn]	$440994\cdot 10^5$	46653.7	20735.0	$440994\cdot 10^3$	466.537	207.350
$d\sigma^B/d\sigma^0$ $[10^{-3}]$	$-8.626\cdot 10^{-4}$ $-8.182\cdot 10^{-4}$	0.05267 0.05024	-1.295 -1.230	$1.235\cdot 10^{-4}$ $-0.076(1)\cdot 10^{-4}$	0.1267 0.1168	-1.421 -1.532
$d\sigma^V/d\sigma^0$ $[10^{-3}]$	$-1.234\cdot 10^{-4}$ $-1.191\cdot 10^{-4}$	-0.01877 -0.01796	-0.005167 -0.004983	-0.004261 -0.004084	-0.2695 -0.2560	-0.2352 -0.2246
$d\sigma^{\rm red}/d\sigma^0$ $[10^{-3}]$	$8.934\cdot 10^{-4}$ $8.169\cdot 10^{-4}$	0.4461 0.4286	-0.3666 -0.3388	0.08860 0.08529	3.317 3.098	2.644 2.290
$d\sigma_{\rm had}/d\sigma^0$ $[10^{-3}]$	$-0.9259\cdot 10^{-4}$ $-1.204\cdot 10^{-4}$	0.4800 0.4609	-1.667 -1.575	0.08446 0.08120	3.175 2.959	0.9880 0.5341
$d\sigma_e/d\sigma^0$ $[10^{-3}]$	0.3114	0.7070	-1.460	0.6862	0.4773	-3.516
$d\sigma_\mu/d\sigma^0$ $[10^{-3}]$	$6.623\cdot 10^{-4}$	0.3273	0.3275	0.09040	1.143	0.6128
$d\sigma_\tau/d\sigma^0$ $[10^{-3}]$	$4.100\cdot 10^{-6}$	0.004869	$-7.525\cdot 10^{-4}$	$3.926\cdot 10^{-4}$	0.2776	0.3265

$\sqrt{s}$	M_Z			500 GeV		
θ	3^o	90^o	177^o	3^o	90^o	177^o
$d\sigma^0/d\Omega$ [pbarn]	5303480	5.61067	2.49363	176398	0.186615	0.0829400
$d\sigma^B/d\sigma^0$ $[10^{-3}]$	0.001685 0.001579	0.03648 0.03537(1)	-3.418 -3.200	0.002188 0.002055	-0.1682 -0.1557	-7.017 -6.589
$d\sigma^V/d\sigma^0$ $[10^{-3}]$	-0.08749 -0.08347	-1.458 -1.375	-1.516 -1.430	-0.4614 -0.4373	-3.715 -3.495	-3.970 -3.734
$d\sigma^{\rm red}/d\sigma^0$ $[10^{-3}]$	1.650 1.562	8.340 7.835	8.001 7.526	4.594 4.289	13.35 12.60	12.84 12.12
$d\sigma_{\rm had}/d\sigma^0$ $[10^{-3}]$	1.565 1.480	6.918 6.495	3.066 2.895	4.135 3.854	9.469 8.944	1.855 1.795
$d\sigma_e/d\sigma^0$ $[10^{-3}]$	0.8128	-0.4993	-6.769	0.5561	-1.954	-10.33
$d\sigma_\mu/d\sigma^0$ $[10^{-3}]$	0.7078	1.943	0.3714	1.378	2.366	-0.3557
$d\sigma_\tau/d\sigma^0$ $[10^{-3}]$	0.04932	1.246	0.9548	0.4787	2.100	1.162

Table 2: Born cross section and relative corrections from hadronic irreducible boxes and vertices, reducible hadronic contributions and their sum, for selected energies and angles. Upper/lower lines: parametrization B/HMNT. Also shown are the corresponding contributions from electrons, muons and τ-leptons.

$\theta = 3^o$	$\sqrt{s}$	1 GeV	10 GeV	M_Z	500 GeV
	$d\sigma^B/d\Omega$	-0.380382	0.000544704	0.0000893354	0.00000386014
had	$d\sigma^{B+\text{red}}/d\Omega$	0.0136085	0.391247	0.0876187	0.00810786
		< 1	0.39	0.0877	0.0081
	$d\sigma^B/d\Omega$	0.0419870	0.00132934	0.0000283258	0.00000100529
μ	$d\sigma^{B+\text{red}}/d\Omega$	0.339976	0.417217	0.0407916	0.00287809
		< 1	0.42	0.0408	0.00288
	$d\sigma^B/d\Omega$	-0.000277434	0.000350300	0.0000118080	0.000000773826
τ	$d\sigma^{B+\text{red}}/d\Omega$	0.00227893	0.00193150	0.00270529	0.000876352
		< 1	$< 10^{-2}$	0.0027	0.00088

$\theta = 90^o$	$\sqrt{s}$	1 GeV	10 GeV	M_Z	500 GeV
	$d\sigma^B/d\Omega$	24.5724	0.591300	0.00204702	-0.000313808
had	$d\sigma^{B+\text{red}}/d\Omega$	232.674	16.0671	0.469946	0.0246035
		234	16.07	0.4701	0.02461
	$d\sigma^B/d\Omega$	12.8008	0.133680	-0.00115553	-0.000171183
μ	$d\sigma^{B+\text{red}}/d\Omega$	160.197	6.08187	0.147046	0.00725789
		160	6.08	0.1470	0.00726
	$d\sigma^B/d\Omega$	0.465857	0.0939460	0.00188681	0.0000195543
τ	$d\sigma^{B+\text{red}}/d\Omega$	2.38272	1.33347	0.0752669	0.00457124
		2	1.33	0.0752	0.00457

Table 3: Corrections from the irreducible boxes (first line), sum of box and reducible contributions (second line) and comparison with [9] (third line), for hadrons, muons and τ-leptons at selcted energies and angles. In the upper table the numbers are in units of 10^2 nbarn, in the lower one in units of 10^{-4} nbarn.

The implementation of these results in a Monte Carlo generator is straightforward and their modular structure should lead to an efficient program. The reducible contribution $d\sigma^{\text{red}}$ can be obtained from the one-loop corrections simply modifying the photon propagators outside the loop according to:

$$\frac{1}{q^2} \to \frac{1}{q^2}\big[1 + \text{Re}\Pi(q^2)\big], \qquad \Pi = \Pi_{\text{had}} + \Pi_e + \Pi_\mu + \Pi_\tau, \tag{54}$$

and adding the terms proportional to $\text{Im}\Pi(s)$ multiplied by the imaginary part of the one-loop result. The irreducible vertex corrections $V(q^2)$ can be directly combined with the Born cross section. All these are one-dimensional functions that can be tabulated once for ever. The irreducible box contribution is decomposedinto terms proportional to $\Pi(s)$ and $\Pi(t)$ plus a remainder characterized by the functions $B(s,t,u)$, $B(s,u,t)$, $B(t,s,u)$ and $B(t,u,s)$. These are obtained through efficient and precise integration routines[5].

[5]available upon request from the authors.

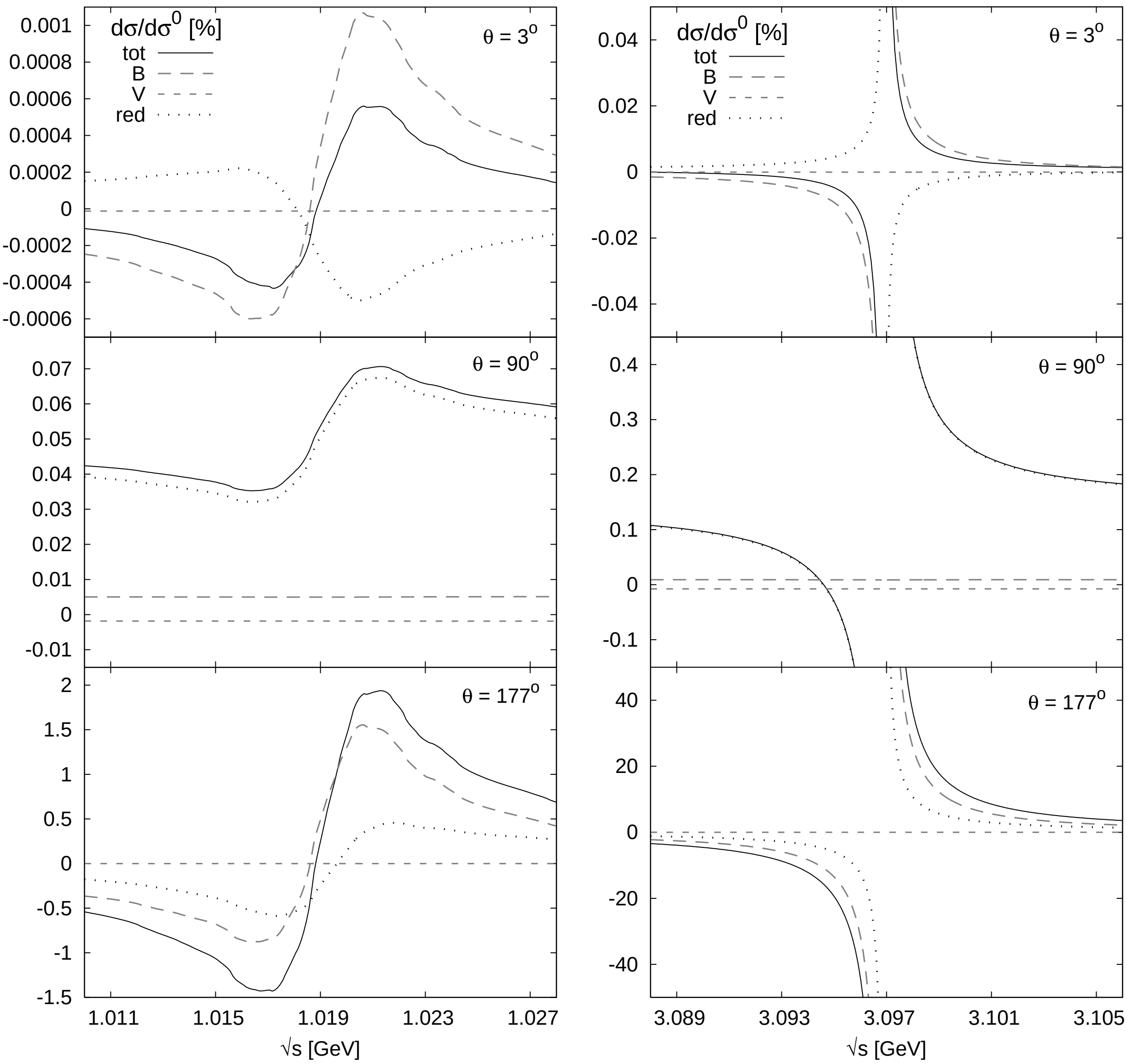

Figure 13: Behaviour of the hadronic corrections around the Φ and the J/Ψ resonances for three characteristic angles.

6 Conclusions

Using published one-loop results, a compact formula has been derived which, in combination with dispersion relations and the by now well-measured R-ratio, can be used to evaluate the hadronic contributions to Bhabha scattering. The same approach is applicable for leptonic contributions, in particular from muons and τ-leptons. The method and result are valid in the limit $m_e^2 \ll s, |t|, |u|$ for arbitrary $R(s)$ and arbitrary $m_{\mu,\tau}^2/s$. Comparing with [9], our numerical results are in perfect agreement for massive leptons, with m_l^2 arbitrary, while for hadronic contributions we observe small numerical differences. In the high energy limit the integrals can be evaluated in analytic form and the results have been compared with those for lepton loops that can be found in the literature. We find that overall size of the corrections, their sign and their angular dependence differ significantly between hadron, muon, τ-lepton and electron contributions. The size of the hadronic corrections varies from a fractional up to several permille. However, these are dominated by the reducible ones, with the irreducible box and vertex terms being typically below one permille. The modular structure of the results allows for a simple implementation into any Monte Carlo generator. For such an implementation, the corrections from virtual plus soft real photon radiation must be complemented by hard real radiation. This part is evidently straightforward, since it involves tree-level diagrams only, with the photon propagator dressed by hadronic vacuum polarization.

Acknowledgments

We would like to thank H. Burkhardt and T. Teubner for providing us with the parametrizations for the function $R(s)$ and A. Penin and T. Teubner for helpful comments. Work supplied by BMBF contract 05HT4VKAI3.

References

[1] A. A. Penin, Phys. Rev. Lett. **95** (2005) 010408 [arXiv:hep-ph/0501120], Nucl. Phys. B **734** (2006) 185 [arXiv:hep-ph/0508127].

[2] Z. Bern, L. J. Dixon and A. Ghinculov, Phys. Rev. D **63** (2001) 053007 [arXiv:hep-ph/0010075].

[3] T. Becher and K. Melnikov, JHEP **0706** (2007) 084 [arXiv:0704.3582 [hep-ph]].

[4] M. Czakon, J. Gluza and T. Riemann, Nucl. Phys. B **751** (2006) 1 [arXiv:hep-ph/0604101];
S. Actis, M. Czakon, J. Gluza and T. Riemann, Nucl. Phys. B **786** (2007) 26 [arXiv:0704.2400 [hep-ph]].

[5] R. Bonciani, A. Ferroglia and A. A. Penin, JHEP **0802** (2008) 080 [arXiv:0802.2215 [hep-ph]], Phys. Rev. Lett. **100** (2008) 131601 [arXiv:0710.4775 [hep-ph]].

[6] R. Bonciani, P. Mastrolia and E. Remiddi, Nucl. Phys. B **661** (2003) 289 [Erratum-ibid. B **702** (2004) 359] [arXiv:hep-ph/0301170], Nucl. Phys. B **676** (2004) 399 [arXiv:hep-ph/0307295]. Nucl. Phys. B **690** (2004) 138 [arXiv:hep-ph/0311145];
R. Bonciani, A. Ferroglia, P. Mastrolia, E. Remiddi and J. J. van der Bij, Nucl. Phys. B **681** (2004) 261 [Erratum-ibid. B **702** (2004) 364] [arXiv:hep-ph/0310333]; Nucl. Phys. B **701** (2004) 121 [arXiv:hep-ph/0405275]. Nucl. Phys. B **716** (2005) 280 [arXiv:hep-ph/0411321].

[7] M. Czakon, J. Gluza and T. Riemann, Phys. Rev. D **71** (2005) 073009 [arXiv:hep-ph/0412164];
R. Bonciani and A. Ferroglia, Phys. Rev. D **72** (2005) 056004 [arXiv:hep-ph/0507047].

[8] N. Cabibbo and R. Gatto, Phys. Rev. **124** (1961) 1577.

[9] S. Actis, M. Czakon, J. Gluza and T. Riemann, Phys. Rev. Lett. **100** (2008) 131602 [arXiv:0711.3847 [hep-ph]]; S. Actis, J. Gluza and T. Riemann, arXiv:0807.0174 [hep-ph].

[10] H. Burkhardt, TASSO-NOTE-192 and privat comunications.

[11] Private communications, routine based on the data compilation of:
K. Hagiwara, A. D. Martin, D. Nomura and T. Teubner, Phys. Lett. B **649** (2007) 173 [arXiv:hep-ph/0611102], Phys. Rev. D **69** (2004) 093003 [arXiv:hep-ph/0312250].

[12] B. A. Kniehl, M. Krawczyk, J. H. Kühn and R. G. Stuart, Phys. Lett. B **209** (1988) 337.

[13] R. W. Brown, R. Decker and E. A. Paschos, Phys. Rev. Lett. **52** (1984) 1192;
M. Bohm, A. Denner, T. Sack, W. Beenakker, F. A. Berends and H. Kuijf, Nucl. Phys. B **304** (1988) 463.

[14] G. J. H. Burgers, Phys. Lett. B **164** (1985) 167.

[15] A. O. G. Källen and A. Sabry, Kong. Dan. Vid. Sel. Mat. Fys. Med. **29N17** (1955) 1;
K. G. Chetyrkin, J. H. Kühn and M. Steinhauser, Nucl. Phys. B **482** (1996) 213 [arXiv:hep-ph/9606230] and references therein